Absorption of Internal Waves by the Benthic Boundary Layer

ERIC D'ASARO[1]

Woods Hole Oceanographic Institution, Woods Hole, MA 02543

(Manuscript received 7 May 1981, in final form 11 January 1982)

ABSTRACT

The interaction of near-inertial velocities with the benthic boundary layer above a flat bottom is investigated using a diagnostic model and a 3-month time series of velocity from a fixed array of current meters. The observed near-inertial motions are assumed to be due to internal waves and diurnal tides. If the vertical wavelength of the internal waves is much larger than the boundary-layer thickness, the turbulent stresses acting on the near-inertial motions and the work done by the stresses on these motions can be computed. The boundary layer is estimated to absorb -0.003 to 0.024 erg cm^{-2} s^{-1} from the near-inertial motions, with one-third coming from the K_1 diurnal tide and the rest from the internal-wave field. This is far less than estimated by Leaman (1976) and suggests that the benthic boundary layer on a flat bottom plays a minor role in dissipating internal-wave energy. This is also much less than the total energy dissipation in the boundary layer, suggesting that the boundary layer is primarily driven by low-frequency motions, not internal waves. A simple slab model with a linearized quadratic drag law qualitatively explains the observed near-inertial velocity structure and energy flux.

1. Introduction

During the last decade great progress has been made in describing the space-time structure of the internal-wave field (Garrett and Munk, 1979; Gregg and Briscoe, 1979). Still elusive, however, is a clear understanding of the dynamics of the internal-wave field and the magnitude and character of its sources and sinks. One possible location of internal-wave generation and/or absorption is the benthic boundary layer. The boundary layer is known to have characteristics distinct from the oceanic interior (Bowden, 1978), and is certainly the site of considerable energy dissipation. How much of this dissipated energy comes from the internal-wave field? Leaman (1976) estimates a net downward energy flux in the internal-wave field of 0.2–0.3 erg cm^{-2} s^{-1} for a 4-day period in the Sargasso Sea. Müller *et al.* (1978), analyzing the IWEX experiment, find a similar asymmetry confined to the near-inertial frequency band. Kundu (1976) finds a somewhat larger net downward flux in the near-inertial band on the Oregon Shelf. One interpretation is that this net downward energy flux results from absorption of near-inertial waves by the benthic boundary layer. Fu (1981), however, proposes an alternative explanation based on the kinematic properties of surface-generated near-inertial waves. This paper will provide a direct estimate of the absorption of near-inertial waves by the benthic boundary layer on a flat abyssal plain in the western North Atlantic.

The structure of the near-inertial motions in the boundary layer is summarized in Section 2. A diagnostic model of the interaction between near-inertial motions and the boundary-layer turbulence is developed in Section 3. This model is used to compute the energy absorbed by the boundary layer from the near-inertial motions in Section 4. A slab model of the boundary layer is used in Section 5 to explore the dynamics of the boundary layer at near-inertial frequencies.

2. Observed inertial motions

This paper will use data from the Benthic Boundary Layer experiment, described more fully by Armi and D'Asaro (1980) and D'Asaro (1980, 1982). A 3-month record (18 May 1977 to 18 August 1977) of velocity and temperature was obtained from a bottom mooring deployed on the flat Hatteras Abyssal Plain. This mooring contained seven VACM current meters from 15 to 85 m above the bottom.

D'Asaro (1982) describes the observed near-inertial structure of the boundary layer (see his Fig. 6). The clockwise inertial energy decreases near the top of the mixed layer with little phase change. Within the mixed layer the phase increasingly leads that in the interior, with a typical difference of 25° between 15 and 85 m.

Below, an analysis of the observed near-inertial structure is presented. This will yield an estimate of

[1] Present affiliation: Applied Physics Laboratory, University of Washington, Seattle WA 98105.

0022-3670/82/040323-14$07.50

the energy transfer between the interior near-inertial motions and the boundary layer. The interpretation of this number depends critically on the origin of the interior near-inertial motions. At the experimental latitude (28.5°N) the inertial and diurnal tidal frequencies both contribute to the near-inertial frequency band.

Fu (1981) analyzed deep current measurements throughout the western North Atlantic and found the observed inertial peaks consistent with a model of the global internal-wave field. Sanford (1975) found near-inertial baroclinic velocities of roughly 1 cm s^{-1} near the ocean bottom in this area. Although no direct evidence is available, these observations strongly suggest that much of the near-inertial energy measured here is due to internal waves.

The K_1 (0.0418 cph) and O_1 (0.0387 cph) tidal frequencies are very close to the inertial frequency (0.0397 cph). With no more than a 92-day record, these differences can only marginally be resolved, with standard spectral analysis. The unaveraged periodogram for the entire record shows peaks at both at the K_1 and O_1 frequencies with energies of about 0.15 and 0.1 cm^2 s^{-2}, respectively. The calculations below will include only superinertial frequencies and exclude the O_1 tidal band. The near-inertial band from 0.04 to 0.049 cph contains about 1 cm^2 s^{-2}. Assuming the energy at the K_1 frequency to be entirely due to the tide, K_1 accounts for about 12% of the energy in this near-inertial band. The rest is assumed to be due to internal waves.

3. Wave interaction with the boundary layer

The above observations indicate a significant interaction between the near-inertial motions and the boundary layer. In the analysis presented below, these motions will be assumed to be linear. For the diurnal tides, this is clearly justified. The long nonlinear interaction times computed for the energy-containing near-inertial waves (McComas, 1977) justify the linearization for the internal waves. McComas's calculations are based on thermocline wave scales. In the deep ocean the wave scales are significantly larger, and the nonlinear interactions much weaker.

Consider a set of linear waves incident on a flat bottom ocean, with a thin turbulent bottom boundary layer. The waves are superimposed on currents with much larger time scales, here called "mean" currents. In the absence of any waves the mean shear within the boundary layer is balanced by the turbulent-stress divergence. The energy to maintain the stresses is drawn from the mean flow. Any wave superimposed on this balance will modulate the stresses. The energy to maintain the stresses may now come partially from the waves as well as from the mean flow. If there are many waves, the energy will be drawn from some unknown combination of these waves and the mean flow. Since the boundary layer is highly nonlinear one should not expect the energy extracted from any given wave to depend solely on the characteristics of that wave; it may also depend on the other waves and on the mean flow.

The following analysis is designed to compute the absorption of energy from linear waves by a turbulent boundary layer. The analysis assumes the waves to be large compared to the boundary layer and uses the observed wave motions at a particular frequency to compute the turbulent stresses acting on these motions. No assumption concerning the source of these stresses is made; they may be due to motions at other frequencies.

Below, the relevant wave and boundary-layer scales will be computed, and the equations of motion simplified for these scales. The resulting equations will be used to interpret the observed structure.

a. Wave scales

The diurnal tidal motions in this area are primarily barotropic (Zetler *et al.*, 1975) and have much larger scales than any near-inertial internal waves. Since the approximations used break down at small scales, the equation scaling will emphasize internal-wave scales.

The vertical scales of internal waves in the thermocline, away from the inertial frequency, are well known (Garrett and Munk, 1979), but those of near-inertial waves, particularly in the deep ocean, are less well characterized. Munk and Phillips (1968) suggest that they may be modeled as horizontally propagating internal-wave modes that are near their northern turning latitude. In such a model the vertical structure of each mode is independent of latitude, so the near-inertial vertical-wavenumber spectrum is determined by the high-frequency (relative to f) wavenumber spectrum at lower latitudes. Fu (1981) shows that this approach accurately models the observed near-inertial energy spectra in the deep North Atlantic. One result of his analysis is that the near-inertial vertical-wavenumber spectrum should be similar to that at higher frequencies, with, however, less energy in the low-mode waves, as these have a more southerly turning latitude. The inverse analysis of the IWEX experiment (Müller *et al.*, 1978), consistent with this prediction, finds little energy at the lowest three modes for near-inertial motions; these modes contain significant energy only at higher frequencies.

The vertical near-inertial-wave scales will be estimated using the GM75 (Garrett and Munk, 1975) wavenumber spectrum with the addition of a low-wavenumber cutoff. The wavenumber spectrum is given by

$$A(\lambda) = \begin{cases} \dfrac{1.5}{[1 + (\lambda - d)]^{2.5}}, & \lambda > d \\ 0, & \lambda < d \end{cases} \quad (1)$$

where $\lambda = \beta/\beta^*$, for vertical wavenumber β, and $\beta^* \equiv j^*\pi N/bN_0$, with $b = 1.3$ km, $N_0 = 3$ cph, $j^* = 6$ and $d = j_p/j^*$. The low-mode cutoff j_p is taken as 3, following Müller *et al.* (1978). Using a local Väisälä frequency $N = 0.45$ cph, the characteristic vertical wavenumber β^* is found to be 2.2×10^{-3} m^{-1} or $(460\ m)^{-1}$. The smallest energetic wavenumber is $j_p/j^*\beta^*$ or $(920\ m)^{-1}$. Integrating (1) shows that 45% of the energy is found at wavenumbers $< \beta^*$, and 90% of the energy is found at wavenumbers $< 4\beta^* = (115\ m)^{-1}$. For a typical mixed-layer height of $H = 20$ m, β^*H has a value of 0.04, with 90% of the wave energy having $\beta H < 0.17$. The boundary layer is thin compared to the vertical scale of the energetic waves.

The interaction of the waves and boundary layer will also be modulated by the horizontal boundary-layer scales. Fu (1981) finds horizontal near-inertial wave scales > 20 km for the energy containing waves. Armi and D'Asaro (1980) find gross boundary-layer characteristics varying on scales $\geq$ 10 km. Both these scales are much larger than the boundary layer height.

b. *Equations of motion*

The horizontal x-momentum equation for a turbulent Boussinesq fluid with no mean velocity on an f-plane can be written

$$\underbrace{\frac{\partial u}{\partial t}}_{\frac{1}{fT}} + \underbrace{\mathbf{u}\cdot\nabla u}_{\frac{u}{fL}} - \underbrace{fv}_{1} = -\frac{\partial P}{\partial x} - \underbrace{\frac{\partial}{\partial z}(\overline{u'w'})}_{\frac{u^{*2}}{fUH}} - \underbrace{\frac{\partial}{\partial x}(u'^2)}_{\frac{u^{*2}}{fUH}\frac{10H}{L}} - \underbrace{\frac{\partial}{\partial y}(\overline{u'v'})}_{\frac{u^{*2}}{fUH}\frac{H}{L}}, \quad (2)$$

where the turbulent stresses have been scaled by values typical of a two-dimensional turbulent boundary layer (Townsend, 1976, p. 290) and the mean density has been absorbed into P. For near-inertial waves interacting with a turbulent boundary layer of typical height ($H = 20$ m), typical wave-velocity ($u = 1$ cm s^{-1}), length ($L = 20$ km) and time ($T = 1/f = 10^4$ s) scales, the following nondimensional numbers are small: $u/fL = 0.005$, $10H/L = 0.01$. The horizontal momentum equations can now be written

$$\frac{\partial u}{\partial t} - fv = -\frac{\partial P}{\partial x} - \frac{\partial \overline{u'w'}}{\partial z}, \quad (3)$$

$$\frac{\partial v}{\partial t} + fu = -\frac{\partial P}{\partial y} - \frac{\partial \overline{v'w'}}{\partial z}. \quad (4)$$

The magnitude of P can be estimated by Fourier-transforming (3) and (4), using $w = \int \hat{w} e^{i(kx+ly+\sigma t)}$, and solving for the kinetic energy above the boundary layer, i.e.,

$$(\sigma^2 - f^2)^2[|\hat{u}|^2 + |\hat{v}|^2] = (\sigma^2 + f^2)(k^2 + l^2)|\hat{P}|^2, \quad (5)$$

so that

$$P = \frac{uL(\sigma^2 - f^2)}{(\sigma^2 + f^2)^{1/2}}. \quad (6)$$

Note that the pressure gradients above the boundary layer become very small near the inertial frequency.

Armi and D'Asaro (1980) conclude that on the time scale of several days or shorter the temperature fluctuations observed at the mooring are due primarily to advection. Turbulent mass transport becomes important only on a longer time scale. With this assumption the appropriate mass conservation equation for the superinertial motion is

$$\rho = \bar{\rho}_z \xi, \quad (7)$$

$$\xi_t = w, \quad (8)$$

where ξ is the vertical displacement and $\bar{\rho}$ the mean density. The nonlinear terms have been eliminated as from (2) above.

The vertical momentum equation can be written

$$\frac{\partial P}{\partial z} = -[\xi_{tt} + N^2\xi] - \left[\frac{\partial}{\partial z}(\overline{w'^2})\right], \quad (9)$$

$$N^2 = -g\frac{\partial(\ln\bar{\rho})}{\partial z}, \quad (10)$$

where N is the Väisälä frequency, Eq. (7) has been used, and the nonlinear and horizontal-stress-divergence terms have been eliminated as from (2) above.

In the absence of turbulent stresses, Eqs. (3), (4), (7), (8) and (9) are the equations for inviscid linear internal waves. For constant N they have solutions of the form $e^{i\beta z}$, where β is the vertical wavenumber. In the presence of stresses the pressure change across

the boundary layer is given by the sum of the two terms in (9). The vertical displacement ξ is strongly constrained by the ocean bottom at $z = 0$ and the internal wave displacements above the mixed layer. The fractional pressure change across the boundary layer of thickness H due to the first term in (9) should thus be similar to that in the inviscid case, βH, and thus be small. The fractional change in pressure due to the second bracketed term in (9) has a magnitude $u^{*2}/(\sigma - f)uL < 10^{-2}$, where (6) has been used to estimate P, and it is supposed that $\sigma > 1.03f$ and $u^* < 0.2$ cm s^{-1}. The fractional change in pressure across the boundary layer is thus small. This results primarily from the large vertical scale of the near-inertial waves, relative to the boundary layer thickness.

For the diurnal tidal motions the above analysis will be valid with the addition of a barotropic forcing term. This can be included in the pressure term of the scaled equations, since it appears in the equations in the same way.

c. Scaled equations

The scaled equations for motions at a near-inertial frequency σ are

$$-i\sigma\hat{u} - f\hat{v} = -\frac{\partial\hat{P}}{\partial x} - \frac{\partial\hat{\overline{u'w'}}}{\partial z}, \tag{11}$$

$$-i\sigma\hat{v} + f\hat{u} = -\frac{\partial\hat{P}}{\partial y} - \frac{\partial\hat{\overline{v'w'}}}{\partial z}, \tag{12}$$

$$\frac{\partial\hat{P}}{\partial z} = 0, \tag{13}$$

$$\frac{\partial\hat{u}}{\partial x} + \frac{\partial\hat{v}}{\partial y} + \frac{\partial\hat{w}}{\partial z} = 0, \tag{14}$$

where the caret denotes a Fourier transform in time only. These equations are appropriate for a thin domain stretching from the ocean bottom ($z = 0$), to just above the boundary layer. Note that the stress terms in (11) and (12) are the components of turbulent-stress divergence with frequency σ, not the total stress divergences.

These equations can be used to evaluate the interaction of the boundary layer and the wave motions at frequency σ. Consider a level z_r above the boundary layer chosen so that the stress terms in (11) and (12) are negligible. Since the pressure is constant across the boundary layer, the pressure terms in (11) and (12) can be evaluated from the velocity field at z_r, so as to obtain equations for the boundary-layer stresses in terms of the velocity field, i.e.,

$$-\frac{\partial\hat{\overline{u'w'}}}{\partial z} = -i\sigma(\hat{u} - \hat{u}_r) - f(\hat{v} - \hat{v}_r), \tag{15}$$

$$-\frac{\partial\hat{\overline{v'w'}}}{z} = -i\sigma(\hat{v} - \hat{v}_r) + f(\hat{u} - \hat{u}_r), \tag{16}$$

where $\hat{u}_r$, $\hat{v}_r$ are velocity components measured at z_r.

Eqs. (15) and (16) state that the presence of boundary-layer stresses leads to different velocities within the boundary layer from those above it, even though the pressure field is the same. They state that *all observed velocity shears within the boundary layer are due to turbulent stresses.* This is the usual assumption in boundary-layer analysis. For low-frequency motions, $\sigma \ll f$, Eqs. (15) and (16) become the steady Ekman-layer equations with a three-way balance of Coriolis force ($f\hat{u}$), pressure gradient ($f\hat{u}_r$) and turbulent stresses (Priestly, 1959, p. 34). For $\sigma \geqslant f$ the additional terms in (15) and (16) must be included.

d. Energy equation

Eqs. (15) and (16) allow the turbulent stresses that act upon the motions at frequency σ to be computed from the velocity field. It is precisely these stresses that may absorb energy from the wave motions, and thus act to dissipate the waves. Multiplying (11), (12) and the Fourier transform of (9) by $\hat{u}^\dagger$, $\hat{v}^\dagger$ and $\hat{w}^\dagger$, respectively, (the dagger denotes complex conjugation), summing the products, adding the complex conjugate of the sum, and using (14) gives an energy equation

$$\mathrm{Re}\{\nabla\cdot(\hat{\mathbf{u}}^\dagger\hat{P})\} = -\mathrm{Re}\left\{\hat{u}^\dagger\frac{\partial}{\partial z}(\hat{\overline{u'w'}}) + \hat{v}^\dagger\frac{\partial}{\partial z}(\hat{\overline{v'w'}}) + \hat{w}^\dagger\frac{\partial}{\partial z}(\hat{\overline{w'^2}})\right\}. \tag{17}$$

Eq. (17) states that, for motions at frequency σ, the energy-flux divergence is equal to the rate of working by the boundary-layer stresses on the velocity field.

In the appendix the work done by the third term on the right-hand side of (17) is shown to be small compared to that done by the first two terms. The turbulent-stress divergences can be evaluated from (15) and (16), which yield

$$\left\{\begin{array}{l}\text{Work per unit volume}\\ \text{per unit time done by}\\ \text{stresses on motions}\\ \text{at frequency } \sigma\end{array}\right\} = (\sigma - f)\,\mathrm{Im}\{\hat{C}(\sigma)\hat{C}_r^\dagger(\sigma)\} - (\sigma + f)\,\mathrm{Im}\{\hat{C}(-\sigma)\hat{C}_r^\dagger(-\sigma)\}, \tag{18}$$

$$\hat{C}_- = (\hat{u} + i\hat{v})/\sqrt{2}, \quad (19)$$

where $\hat{C}(\sigma)$ is a complex velocity vector, corresponding to clockwise motion for positive σ and anticlockwise motion for negative σ. $\hat{C}_r(\sigma)$ is evaluated at the reference height z_r, above the boundary layer.

4. Interpretation of near-inertial observations

a. General features

The observed near-inertial motions have less energy within the mixed layer than in the interior. Eqs. (15) and (16) require that all differences in velocity be due to turbulent stresses. The observations thus require turbulent stresses to fill the mixed layer, assuming no turbulent stresses in the interior. Note that a random, statistically steady stress field will have an average inertial component of zero and thus will not affect the near-inertial energy level. At any time such a stress field is as likely to increase the local near-inertial amplitude as to decrease it. Consistently less near-inertial energy within the mixed layer therefore indicates a variation of the boundary layer stresses that is locked in phase with the near-inertial motions, i.e., the boundary-layer stresses are modulated by the near-inertial wave motions.

Eq. (17) gives the energy absorbed by the boundary layer from the near-inertial motions. Note that the presence of stresses alone does not lead to energy absorption. For this the stresses must be correlated with the motion so that work is done. Eq. (18) expresses this same energy absorption as the sum of terms involving the clockwise and anticlockwise components of the velocity field at frequency σ. Each term is proportional to the quadrature spectrum of the motion within the boundary layer with that at some reference level outside the boundary layer. The quadrature spectrum can be expressed as

$$\mathrm{Im}\{\hat{C}\hat{C}_r^\dagger\} = |\hat{C}||\hat{C}_r|\gamma \sin\theta, \quad (20)$$

where γ and θ are the coherence and phase of the boundary-layer velocity with respect to the reference velocity. Since $0 < \gamma < 1$, the sign of the energy transfer between the wave velocities and the turbulent stresses is determined by the sign of the phase, as summarized in Table 1. These results, for the case of energy absorption alone, have been derived by Munk *et al.* (1970) for a laminar Ekman layer. Their results are here shown to be determined on purely energetic grounds.

The near-inertial clockwise velocities in the boundary layer lead those in the interior. According to Table 1 this implies energy absorption by the boundary layer from internal-wave motions with $\sigma > f$, and/or energy flux into motions with $\sigma < f$. Note that although the turbulent stresses fill the mixed layer, they only exchange energy with the waves in the lower part of the mixed layer.

TABLE 1. Energy flux and boundary layer phase.

Clockwise motion	
$\sigma > f$	$\sigma < f$
B.L. leads → absorption B.L. lags → production	B.L. leads → production B.L. lags → absorption
Anticlockwise motion	
all σ	
B.L. leads → absorption B.L. lags → production	

Lead and lag are relative to the direction of rotation.

b. Energy flux calculation

The total work per unit area per unit time, $\Pi(\sigma)$, done by the boundary-layer stresses on the motions at frequency σ is found by integrating (18) across the boundary layer. This yields

$$\Pi(\sigma) = \int_0^{z_r} \mathrm{Im}\{(\sigma - f)\hat{C}(\sigma, z)\hat{C}^\dagger(\sigma, z_r)\}dz - \int_0^{z_r} \mathrm{Im}\{(\sigma + f)\hat{C}(-\sigma, z)\hat{C}^\dagger(-\sigma, z_r)\}dz. \quad (21)$$

Eq. (21) is used below to compute the flux of near-inertial wave energy into the benthic boundary layer.

For near-inertial motions the spectral estimates $\hat{C}(\sigma, z)$ in (21) must be evaluated with a high-frequency resolution to resolve $\sigma - f$. $\hat{C}(\sigma)$ is therefore computed for each instrument using a 1024-element Fourier transform acting on a single 92-day Hamming-windowed piece (Harris, 1978). The raw data are averaged and subsampled over 127.5 min before Fourier-transforming, resulting in a variance reduction of approximately 5% at 0.05 cph. This processing yields estimates of $\hat{C}(\sigma)$ with a frequency resolution of $\sim 0.01f$. For a given instrument pair $\mathrm{Im}\{(\sigma - f)\hat{C}_1\hat{C}_2^\dagger\}$ is computed for each spectral estimate; these products are then averaged over frequency to increase the statistical reliability of the estimate. This processing yields spectral averages at a fixed height off the bottom and ignores any variations in mixed-layer height. For a record of only 92-days length this is unavoidable. The calculation also ignores any Doppler-shifting of the wave frequency by the mean current.

The integrands in (21) are functions of both frequency and the pair of instruments used. The frequency dependence will be examined first. In Fig. 1b the reference level z_r is chosen as 55 m and the energy

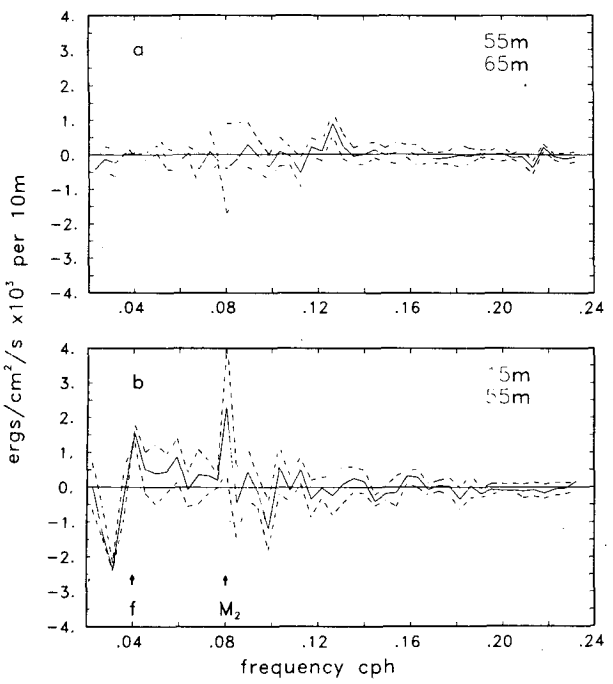

FIG. 1. Energy-absorption density by turbulent boundary layer as computed from Eq. (21) for the clockwise velocity component. The 95% confidence limits computed from phase confidence limits are shown as dashed lines. (a) Reference instrument at 65 m, z = 55 m; (b) reference instrument at 55 m, z = 15 m.

flux resulting from the clockwise term in (21) is plotted for z = 15 m as a function of frequency. The solid line shows the results; the dashed lines give 95% confidence limits computed using the phase confidence limits given by Koopmans (1974, p. 285). The computed energy flux is indistinguishable from zero at frequencies > 0.08 cph. Some energy absorption is indicated at the M_2 tidal frequency. Near the inertial frequency significant energy absorption is indicated for $\sigma > f$; significant production of energy is indicated for $\sigma < f$. Frequencies below 0.02 cph are not well behaved; the magnitude of the energy transfer varies widely with frequency and details of the calculation procedure. They are not shown in Figure 1.

Fig. 1a shows the same computation with z_r = 65 m, z = 55 m. Both these levels are above the boundary layer and as expected there is no energy absorption indicated. The same calculation for the anticlockwise term in (21) shows a weak pattern of energy absorption within the boundary layer and near the inertial frequency.

The integration required by (21) is shown in Fig. 2 for two near-inertial frequency bands. The results are tabulated in Table 2. Fig. 2a shows the integration of the clockwise term for a band extending from the inertial frequency 0.04 cph to 0.069 cph. Each curve in Fig. 2a is a plot of the clockwise integrand from (21), i.e., the energy flux per unit volume, as a function of z for a fixed reference height z_r. The area under each curve gives the energy flux per unit area. The solid vertical lines are selected 95% confidence limits. Fig. 2a indicates significant energy absorption for $z < 20$ m for all reference levels. The double diagonal line, a rough average over all reference levels, yields an energy absorption rate of 0.015 ergs cm^{-2} s^{-1}.

Notice, however, that a large contribution to the integral occurs for $z < 15$ m, where there are no data. Fortunately, the contribution from this region can be bounded by noting that the ordinate in Fig. 2a is a quadrature spectrum, which, according to Eq. (20), is bounded above by $|(\sigma - f)\hat{C}(\sigma, z) \times C^{\dagger}(\sigma, z_r)|$. Estimating this by $(\sigma - f)|\hat{C}(\sigma, z_1)|^2$, z_1 = 15 m, yields a maximum value of the ordinate of 0.018 erg cm^{-2} s^{-1} per 10 m. If the solid line in Fig. 2a is bent at z_1 = 15 so that it intersects 18 at z = 0, an estimate of 0.024 erg cm^{-2} s^{-1} for the energy absorption is found. The region below 15 m could also contribute negatively. If the double solid line in Fig. 2a is bent downward at z = 15 to intersect −18 at z = 0, a net energy production of 0.003 results. These bounds are probably overestimates since $|\hat{C}(\sigma, z)|^2$ will continue to decrease below 15 m. This is apparent in the data of Weatherly and Wimbush (1980; M. Wimbush, personal communication). The phases are also unlikely to be 90°.

Fig. 2c is the same as Fig. 2a but for a narrower frequency band. The boundary-layer signal is somewhat stronger for this band, with larger phases and coherences, and less error. A similar error analysis yields 0.006 erg cm^{-2} s^{-1} with bounds of 0 and 0.009 erg cm^{-2} s^{-1}.

The calculation does not resolve the anticlockwise energy transfer (Figs. 2b, 2d). As discussed by Spencer *et al.* (1981), the instrument at 45 m is believed to exhibit a directional bias of up to 10° relative to the instruments at 55 and 65 m for unknown reasons. The peak at 45 m in Fig. 2b is likely due to this effect. It appears only in the anticlockwise calculation, on account of the small anticlockwise phases. Without this peak, the area under the curves in Fig. 2b, between 15 and 25 m, is only 0.001 erg cm^{-2} s^{-1}, with bounds for the total area, 0–25 m, of −0.01 to 0.017 erg cm^{-2} s^{-1}. The anticlockwise energy transfer in Fig. 2d is resolved even more poorly.

c. Internal-wave-energy absorption

The above calculation yields the rate of energy absorption from near-inertial motions by the boundary layer. As shown in Table 2, there is most likely a net absorption of energy from the near-inertial clockwise motions. The energy flux from the anti-

clockwise motions is unresolved. The dominant errors are due to the lack of measurements below 15 m and the finite record length.

The observed near-inertial motions are the sum of internal-wave and diurnal-tidal motions. Examination of the unaveraged integrands of (21) suggests that the K_1 tidal frequency contributes roughly one-third of the calculated clockwise energy absorption. Assuming that all of the calculated energy absorbed at this frequency comes from the K_1 tide, the remaining two-thirds of the total near-inertial energy absorption (0.01 erg cm^{-2} s^{-1}) is drawn from the internal wave field.

The above calculation does not resolve the flux of energy from the anticlockwise motions. As noted by D'Asaro (1982) and Fu (1981), the near-inertial anticlockwise motions contain far more energy than would be predicted by internal wave theory. This

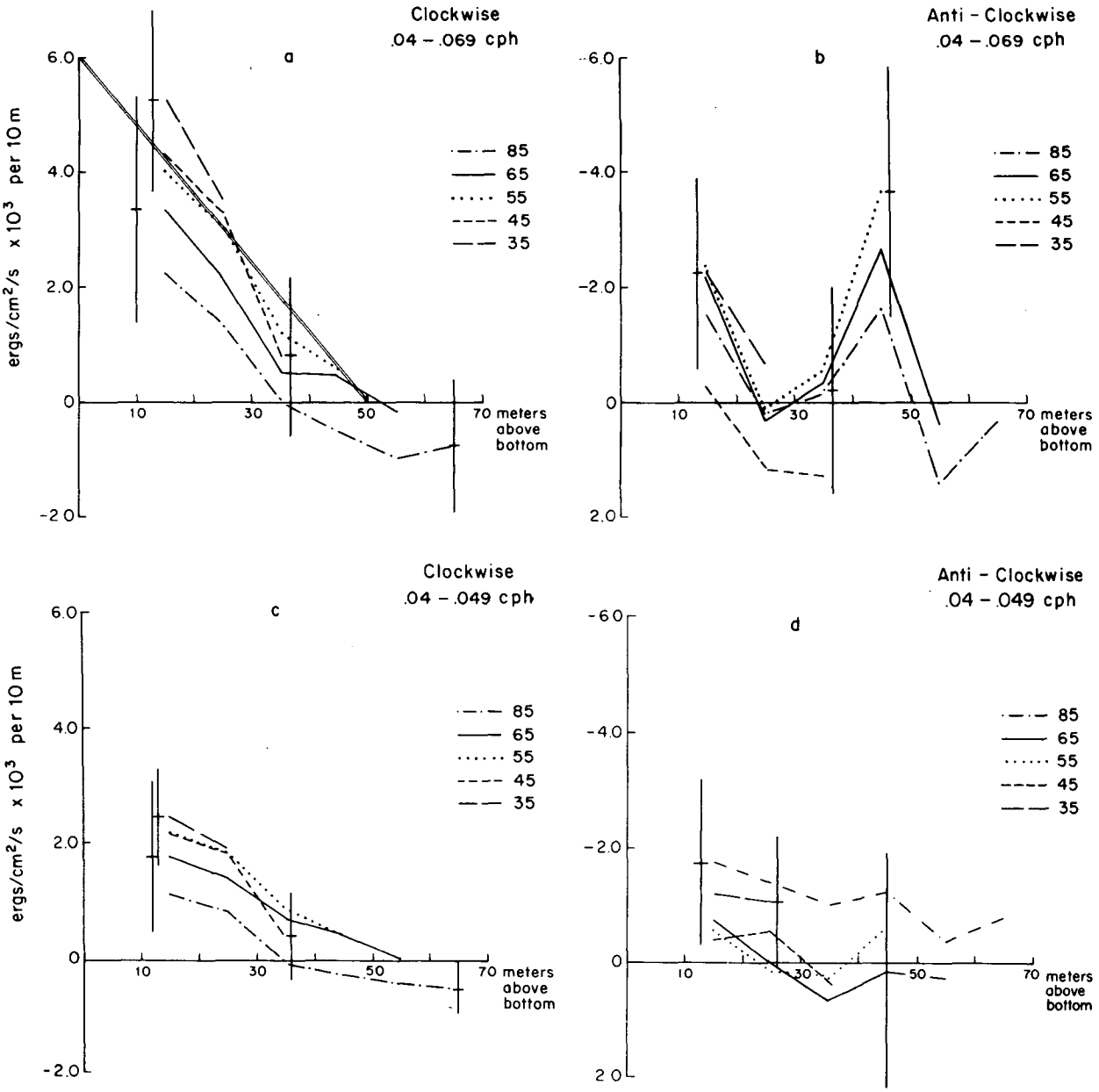

FIG. 2. Computation of near-inertial-energy-absorption rate per unit area by boundary layer using Eq. (21). Each figure shows an integrand of (21) versus height for five different reference levels, 35 to 85 m. The area under each curve gives the estimated energy absorption. The clockwise (2a and 2c) and anticlockwise (2b and 2d) contributions are shown for two near-inertial frequency bands.

TABLE 2. Results.

	0.04–0.069 cph	0.04–0.049 cph
Absorption of energy (ergs cm^{-2} s^{-1})		
Clockwise	0.015	0.006
	−0.003, 0.024	0, 0.009
Anticlockwise	—	—
	−0.010, 0.017	−0.003, 0.005
Downward energy flux (ergs cm^{-2} s^{-1})	0.35	0.12
Reflection coefficient	0.97	0.97
	1.01, 0.95	1.00, 0.95
Clockwise relaxation time (days)	2.5	5.5
H = 20 m	−12.7, 1.6	∞, 3.6

suggests that these motions are not due to internal waves, and that the associated energy flux should not be included in the internal-wave energy budget.

The above calculation suggests an energy flux into the subinertial motions, as shown in Fig. 1b. The change in the sign of the computed energy flux at the inertial frequency is due to the change in sign of $(\sigma - f)$ in Eq. (21); the sign of the relative phase of the boundary-layer and interior motions remains unchanged. Motions with $\sigma \ll f$ are believed to be highly nonlinear and quasi-geostrophic (Rhines, 1979); motions with $\sigma > f$ are believed to be linear internal waves. The dynamics of slightly subinertial motions is unclear. Since the calculation used above assumes a linear momentum equation, it may not correctly estimate the energy flux for $\sigma < f$. The calculation also assumes no mean velocity. Doppler-shifting of the wave frequency by the mean velocity will result in some superinertial wave energy at subinertial frequencies. The calculation will compute the wrong energy flux for these waves. The computed energy flux at slightly subinertial frequencies will not be included in the internal-wave energy budget.

Only the calculated energy flux from near-inertial clockwise motions will be used in the following calculations. This should yield the best estimate of the effect of the benthic boundary layer on the internal-wave field. Including the anticlockwise or subinertial energy absorption in the internal-wave energy budget would have a significant effect on the estimated energy fluxes (cf. Table 2, Fig. 1).

d. Results of calculations

The calculated energy absorption rates for the near-inertial motions are shown in Table 2. Over the period of this experiment the boundary layer absorbs roughly $\Pi = 0.01$ erg cm^{-2} s^{-1} from the near-inertial wave field. This is a net flux. Although the generation of internal waves may be occurring (Townsend, 1965), absorption of near-inertial energy generated elsewhere dominates, resulting in a net absorption of near-inertial internal waves.

The calculated clockwise-energy absorption rate has been used to compute an internal-wave reflection coefficient

$$|R(\sigma)|^2 = \frac{F_+(\sigma)}{F_-(\sigma)} = 1 - \frac{\Pi(\sigma)}{F_-(\sigma)}, \tag{22}$$

where F_+ and F_- are the upward and downward internal-wave energy fluxes, respectively. The downward energy flux F_- can be estimated from

$$F_- = C_g \frac{E(\sigma)}{2} = \frac{\sigma^2 - f^2}{\sigma\beta} \frac{E(\sigma)}{2}, \tag{23}$$

where C_g is the vertical component of internal-wave group velocity (Lighthill, 1978). $|R|^2$ is assumed to be close to 1 so that roughly half the internal-wave energy $E(\sigma)$ is propagating downward. Eq. (23) is evaluated with the same technique used to evaluate the integrands of (21). A value of $\beta = \beta^* = (460\ \text{m})^{-1}$ gives approximately the same energy flux as the entire spectrum (1). The resulting values of F_- and $|R|^2$ are shown in Table 2. The reflection coefficient is roughly 0.97 so that 3% of the wave energy is absorbed in each reflection.

Another useful measure of the energy absorption rate is the boundary layer relaxation time

$$\tau_R = \frac{E(\sigma)\, H}{\Pi(\sigma)}, \tag{24}$$

which gives the time required for the observed energy absorption rate to reduce the observed kinetic energy within the boundary layer of height H to zero, if there were no energy input. Unlike the reflection coefficient, τ_R depends only on boundary-layer properties and does not require any knowledge of the wave properties. Evaluating (24) yields relaxation times of several days.

5. Slab model of boundary layer

In the previous section the absorption of internal-wave energy by the benthic boundary layer was computed. The physics responsible for this absorption is examined below. A simple slab model with a linearized quadratic drag law will be shown to account for most of the observed internal-wave/boundary-layer interactions. With the exception of the computed reflection coefficient, the model should also apply for the tidal motions.

a. Equations

Consider a mixed layer of height H, uniform in velocity and density above a flat bottom, and underlying a region with constant buoyancy frequency N (Fig. 3). A constant velocity U is imposed in the $+x$ direction. Above the mixed layer the fluid is inviscid. The observed mixed layers are generally capped by a density change of order $g\Delta\rho/\rho \approx N^2H$. Since $\beta H \ll 1$ for vertical wavenumbers β, typical of the deep ocean, this density step is dynamically insignificant (D'Asaro, 1978), and is not included in the model.

The observations presented by D'Asaro (1982) clearly indicate the presence of turbulent stresses throughout the mixed layer. Their structure within the mixed layer is less clear, particularly as no measurements were taken below 15 m above the bottom. An integral model of the boundary layer will thus be used. Within the mixed layer the turbulent stresses τ are assumed to decay linearly from their bottom value τ_0 to zero at $z = H$. τ_0 acts to oppose the instantaneous mixed layer velocity and has magnitude $|\tau_0| = u^{*2} = C_DS^2$, where S is the instantaneous mixed-layer speed. The typical inertial velocities (1 cm s^{-1}) are much less than the typical mean velocities (7 cm s^{-1}), so that the drag law can be linearized. The linearized Boussinesq equations for the perturbation quantities in the mixed layer are

$$\frac{\partial u}{\partial t} - fv = -\frac{\partial P}{\partial x} - 2ru, \tag{25}$$

$$\frac{\partial v}{\partial t} + fu = -\frac{\partial P}{\partial y} - rv, \tag{26}$$

$$\frac{\partial u}{\partial x} + \frac{\partial v}{\partial y} + \frac{\partial w}{\partial z} = 0, \tag{27}$$

where $r = C_DU/H$ results from linearizing the drag law, and P denotes the pressure divided by density. Within the mixed layer u, v, P and $\partial w/\partial z$ are constant and since $w(0) = 0$, $\partial w/\partial z = w(H)/H$. The mixed layer velocities are completely determined by the value of P at $z = H$. This model is similar to that of Fu (1981), although he does not include a mean current.

In the interior, Eqs. (25)–(27) apply with $r = 0$ and

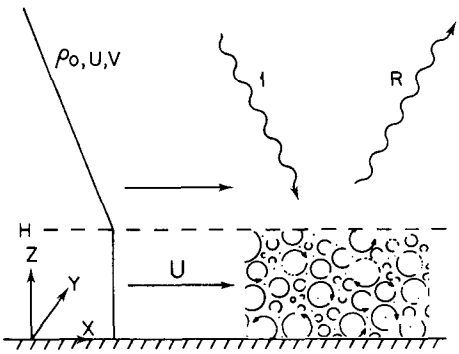

FIG. 3. Slab model of internal-wave interaction with boundary layer. The mixed layer is uniform in density and velocity with a drag applied to it at the ocean bottom. The interior is inviscid, with constant N, and a downward-propagating wave reflecting from the mixed layer.

$$\frac{\partial w}{\partial t} + N^2\xi = -\frac{\partial P}{\partial z}, \tag{28}$$

$$\frac{\partial \xi}{\partial t} = w. \tag{29}$$

These are the well-known internal-wave equations (Garrett and Munk, 1979). Assuming that all quantities vary as $e^{i(kx+ly-\sigma t)}$ interior equations have a solution of the form

$$P = e^{i\beta z} + Re^{-i\beta z}, \tag{30}$$

$$\beta^2 = (k^2 + l^2)(N^2 - \sigma^2)/(\sigma^2 - f^2). \tag{31}$$

This corresponds for $\beta > 0$ to a downward propagating internal wave of unit amplitude and an upward propagating wave of amplitude R. The equations can be solved by requiring P and w to be continuous at $z = H$.

Solving the mixed layer and interior equations separately for $w(H)$ in terms of P yields

$$\frac{1-R}{1+R} = -\frac{\sigma}{\beta H(\sigma^2 - f^2)} \frac{\sigma^2 - f^2 - 2r^2 + 3ir\sigma}{r(1 + \sin^2\theta) - i\sigma}, \tag{32}$$

where $\sin\theta = l/(k^2 + l^2)^{1/2}$.

Solving (25) and (26) for $|u|^2 + |v|^2$ in terms of P with and without r yields the ratio of kinetic energy within the mixed layer to that immediately above it:

$$\frac{(|u|^2 + |v|^2)_{ML}}{(|u|^2 + |v|^2)_{INT}} = \frac{(\sigma^2 - f^2)^2}{(\sigma^2 + f^2)} \frac{\sigma^2 + f^2 + r^2(1 + 3\sin^2\theta) - 2rf\sin\theta\cos\theta}{(\sigma^2 - f^2 - 2r^2)^2 + 9r^2\sigma^2}. \tag{33}$$

A similar calculation yields the cross-spectra for the clockwise component of motion

$$C_{ML}(\sigma)C^{\dagger}_{INT}(\sigma) = \frac{\sigma + f - r\sin\theta\cos\theta + ir(1 + \sin^2\theta)}{(\sigma - f)[\sigma^2 - f^2 - 2r^2 + 3ir\sigma]} \frac{(k^2 + l^2)}{2} |P|^2. \tag{34}$$

The relaxation time τ_R defined by (24) can be computed by forming an energy equation yielding

$$\tau_R = \frac{1}{2r}\frac{\sigma^2 + f^2 - 2rf\sin\theta\cos\theta + r^2(1 + 3\sin^2\theta)}{\sigma^2 + f^2 + \sigma^2\cos^2\theta + f^2\sin^2\theta + 2r^2(1 + \sin^2\theta)}. \quad (35)$$

b. Results

The slab model has one parameter, $r = C_D U/H$. Using $U/u^* = 32$, $H = 20$ m, $U = 7$ cm s^{-1} yields $r = 3.4 \times 10^{-6}$ s^{-1}. Note that $r \ll f$. For a given incident internal wave specified by a frequency σ, a vertical wavenumber β and a propagation direction θ, the model predicts the boundary-layer velocity field, and a wave reflection coefficient R. Since both the interior velocity field at $z = H$ and the boundary layer velocity field are determined by the pressure at $z = H$, all quantities involving just these velocities are independent of the vertical wavenumber of the wave.

Fig. 4a shows the relaxation time $\tau_R(\sigma)$ from Eq. (35). It is somewhat larger than 1 day, and roughly independent of frequency and wave direction. This value is smaller by roughly a factor of 2 than the value calculated from the current-meter data (Table 2). From Eq. (35) τ_R is seen to vary roughly as $1/(3r)$ for $\sigma \approx f$ and $r/f \ll 1$. This result can be simply derived by forming an energy equation from (25)–(29); the energy absorption rate is seen to be $r[2|u|^2 + |v|^2]$. If $|u|^2 \approx |v|^2$ the energy absorption rate is $3r\frac{1}{2}(|u|^2 + |v|^2)$, the energy density is $\frac{1}{2}(|u|^2 + |v|^2)$ so $\tau_R = 1/(3r)$.

Fig. 4b shows the ratio of horizontal kinetic energy in the mixed layer to that in the interior at $z = H$ [Eq. (33)]. The results are independent of direction, but strongly frequency-dependent. For $\sigma > 1.3f$ these energies are nearly the same; for $\sigma < 1.3f$, the boundary-layer energy decreases, reaching zero at $\sigma = f$. This behavior is consistent with the observations (D'Asaro, 1982) which show significantly less inertial energy in the bottommost instruments only for σ near f.

A scale analysis of the momentum equations (25) and (26) explains the special significance of the inertial frequency. Within the boundary layer a balance of inertial, frictional and pressure forces exists. The magnitude of the pressure forces is $u_r(\sigma - f)$ by (6), where u_r is the typical velocity above the boundary layer. For $\sigma - f \gg r$ the inertial forces have magnitude σu. The frictional forces, of magnitude ru, are much smaller since $r \ll f$. The inertial and pressure forces balance, just as in the interior, and the velocities inside the boundary layer are the same as above it. The relative magnitudes of the terms in (25) for $\sigma - f \gg r$ are

$$\left.\begin{array}{l} \underbrace{-i\sigma u - fv}_{} = \underbrace{-ikP}_{} \quad \underbrace{-2ru}_{} \\ (\sigma - f)u \quad = (\sigma - f)u_r \quad ru \end{array}\right\}. \quad (36)$$

For $\sigma - f \approx r$ this balance can no longer hold and the frictional terms become important. For $\sigma - f \ll r$ they become dominant and a new balance exists

$$\left.\begin{array}{l} \overbrace{\qquad}^{} \quad \overbrace{\qquad}^{} \quad \overbrace{\qquad}^{} \\ ru \quad = (\sigma - f)u_r \quad ru \end{array}\right\}. \quad (37)$$

The boundary layer velocity u is much smaller than the interior velocity u_r, their ratio being roughly $(\sigma - f)/r$, as in (33). In physical terms, the drag forces are small and only become important near the inertial frequency where the inertial forces and pressure gradients in the waves become small.

Figs. 4c and 4d show the relative phase of the boundary-layer and interior velocities for clockwise and anticlockwise components, respectively. These phases are small except near the inertial frequency, for the reasons discussed above. The model clockwise boundary-layer phase leads the interior phase, consistent with the observations. The anticlockwise phase is highly dependent on θ. Since the oceanic internal-wave field will consist of waves with many different θ, the average anticlockwise phase should be zero, again consistent with the observations.

Fig. 4e shows the model reflection coefficient $|R|^2$ as a function of frequency. Unlike the quantities shown in Figs. 4a–4d, $|R|^2$ depends on the vertical wavenumber of the incoming wave. A value of $\beta = (460\text{ m})^{-1}$ is used, the same value as in Table 2. The predicted reflection coefficient is significantly less than 1 only near the inertial frequency. It achieves a minimum value of ~ 0.9, at $\sigma \approx 1.1f$, before rising to 1 at $\sigma = f$. The value of $|R|^2$ computed from the data is consistent with this behavior, showing a significant absorption only near the inertial frequency, with a value of $|R|^2 \approx 0.97$ (Table 2, Fig. 3). The predicted behavior of $|R|^2$ can be explained by noting that

$$|R|^2 = 1 - \frac{H}{\tau_R}\frac{E_{ML}}{E_{INT}}\frac{2}{C_g} \quad (39)$$

according to (22)–(24). From Fig. 4a, τ_R can be considered constant; E_{ML}/E_{INT} is shown in Fig. 4b. For $\sigma \gg f$, $E_{ML}/E_{INT} \approx 1$; C_g, however, varies as $\sigma^2 - f^2$ so that $1 - |R|^2 \approx 1/(\sigma^2 - f^2)$. For $\sigma - f \ll r$, E_{ML}/E_{INT} decreases as $(\sigma^2 - f^2)^2$ [Eq. (33)], so $1 - |R|^2 \approx (\sigma^2 - f^2)$. A minimum value of $|R|^2$ therefore occurs for $\sigma \approx f + r$. In physical forces, $|R|^2$ is near 1 for $\sigma \gg f$ because the frictional terms are small. $|R|^2$ decreases as σ approaches f because the group velocity decreases and the small frictional forces have more time to act on the wave. Very near

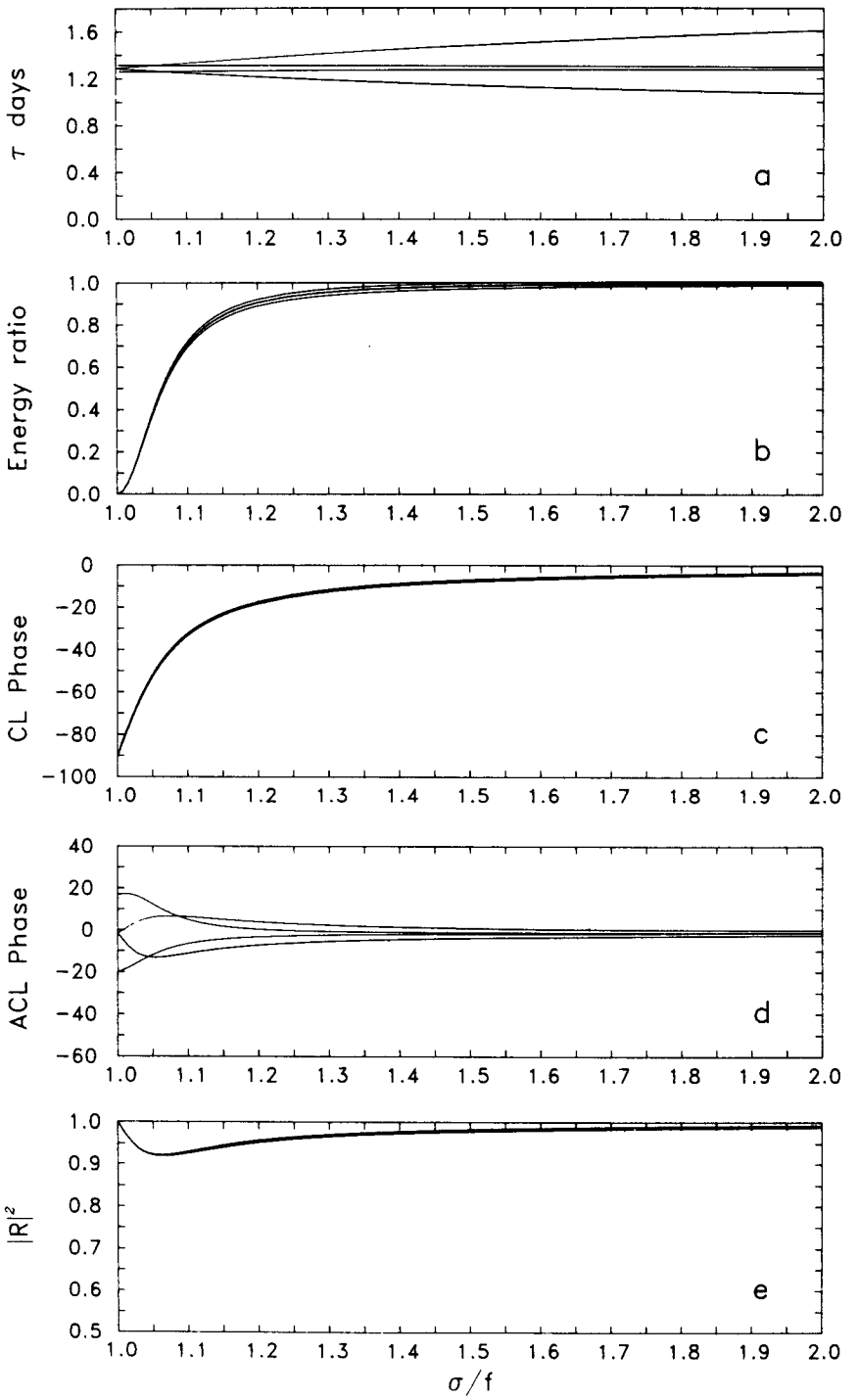

FIG. 4. Slab model results plotted versus frequency, for wave orientations $\theta = -90°, -45°, 0°, 45°, 90°$ and $r = 3 \times 10^{-6}\ s^{-1}$. (a) Relaxation time [Equation (35)]; (b) ratio of horizontal-kinetic-energy density within mixed layer to energy above mixed layer [Equation (33)]; (c) phase of clockwise velocity within mixed layer relative to interior [Equation (34)]; (d) as in 2c except for anticlockwise velocity; (e) reflection coefficient for wave energy assuming $\beta = (460\ m)^{-1}$ [Equation (32)].

f, the frictional forces decrease the boundary-layer velocities and $|R|^2$ increases toward 1.

The least-known parameter in the above model is β, the vertical wavenumber. Since the group velocity is proportional to β^{-1}, $|R|^2$ is highly dependent on β [Eq. (39)]. Longer waves have a faster group ve-

locity and are absorbed less, while short waves, conversely, are absorbed more strongly. Thus, although the boundary layer may not strongly absorb the internal-wave field as a whole, its effect may be much stronger on the shorter, slower internal waves.

Although this model accounts qualitatively for much of the observed near-inertial response of the boundary layer, it predicts about double the observed energy absorption. This is reflected in a smaller relaxation time, smaller reflection coefficient and larger clockwise phase. The observed near-inertial response shows considerable structure within the boundary layer, which is not modeled here. This may explain the difference between the model and the observations.

6. Discussion

The above calculation of near-inertial energy flux into the boundary layer is subject to several uncertainties not included in the error bounds. The array used in this experiment is, as mentioned above, too short to provide any vertical-wavenumber estimates for the internal-wave field. The calculation provides an estimate of energy flux from the near-inertial motions into the boundary layer, but does not require the near-inertial motions to be related to the internal-wave field in midwater. Leaman (1976) finds a near-bottom peak in internal-wave energy within a few hundred meters of the bottom in this area. This suggests that the dynamics of the near-bottom internal wave field might be different from that in midwater, so that flux measured here might not be relevant to the energy budget of the midwater internal-wave field. A related source of uncertainty results from the division of the energy flux into clockwise and anticlockwise sources. As discussed above, only the flux resulting from the clockwise near-inertial motions is used in the calculation. Similarly, the calculation indicates a significant energy flux out of the boundary layer at slightly subinertial frequencies. This flux has, perhaps incorrectly, not been included in the estimated near-inertial wave energy flux. Finally, the fraction of the energy absorption due to the diurnal tide has been only crudely estimated. Statistical estimates of these uncertainties are difficult to form, but they probably will not change the sign or general magnitude of the computed flux.

The estimated flux of energy from the internal-wave field given above includes only contributions from the near-inertial motions. Energy absorption from frequencies > 0.07 cph has not been included, as the calculated absorption is below the statistical noise. The model presented in Section 5 suggests that for $\sigma \gg f$ the absorption of internal waves by the boundary layer can be modeled using a constant relaxation time τ_R acting on the wave kinetic energy. Using $\tau_R = 2$ days, a boundary layer height $H = 20$ m, and an energy of 0.7 cm^2 s^{-2} for the band 0.07–0.45 cph, an energy flux of 0.008 erg cm^{-2} s^{-1} is obtained, which adds significantly to the total absorption of internal wave energy.

The calculation presented here claims to estimate only the energy absorbed from the interior near-inertial motions. The calculated energy fluxes do not represent the entire energy flux into the boundary layer. Eq. (21) could also be applied to the estimate of the energy flux from the geostrophic motions. In this case the integrand is just the pressure gradient times the down-pressure velocity, and is, for small angles, proportional to the veering of the velocity. The 1-day mean veering observed between 15 and 25 m is, at most, a few degrees, far less than the observed errors in direction (Armi and D'Asaro, 1980, plate 1), or the veering observed by Weatherly (1972) closer to the bottom. Thus the absorption of energy from the low-frequency velocity cannot be estimated using Eq. (21) and these data. The absorption of energy from near-inertial motions can be estimated since it occurs in the outer part of the boundary layer. The greater thickness of the inertial boundary layer is consistent with the resonant response of rotational boundary layers at the inertial frequency (Greenspan, 1968).

The energy absorption calculated here, when integrated over all frequencies, should equal the total rate of turbulent-kinetic-energy dissipation in the boundary layer. The depth profile of energy absorption from any particular frequency need not be similar to the turbulent-kinetic-energy-dissipation profile, since significant transport of energy between frequencies and between depths certainly occurs within the boundary layer.

The relative importance of the near-inertial and low-frequency motions in the boundary-layer energetics can be estimated by computing the energy fluxes from these two sources. The low-frequency, turbulent-kinetic-energy production in a boundary layer is of order $U_1 u^{*2}$ (Tennekes and Lumley, 1972, p. 163) or 0.38 erg cm^{-2} s^{-1}. This is much more than the energy absorbed from the near-inertial motions. The boundary layer is thus driven primarily by the low-frequency geostrophic velocities; the inertial motions only modulate it.

The flux of internal wave energy into the boundary layer is calculated here for one location averaged over three months. The model presented in Section 5 suggests that this flux should be proportional to the near-bottom current speed. This predicts considerably larger absorption of internal-wave energy to the north of this site where the currents are larger (Schmitz, 1976) and considerably less absorption for regions of low near-bottom speeds. The calculation is probably not relevant to regions of significant bottom slope or rough topography where the kinematics of the internal-wave field are more complex (Phillips,

1977, chap. 5). This calculation *cannot* be used to estimate fluxes into or out of the internal wave field over rough topography.

Previous observations of near-inertial waves have shown a net downward energy flux (Müller *et al.*, 1978; Leaman, 1976). If the difference between downward- and upward-going energy is attributed to absorption in the boundary layer a reflection coefficient $|R|^2 \approx 0.5$ is predicted (Leaman, 1976). The analysis presented here is not consistent with such a small value of $|R|^2$ and suggests that an alternate explanation, such as that advanced by Fu (1981), is more nearly correct.

The absorption of internal-wave energy by the boundary layer will act as a net sink of energy for the internal-wave field. Assuming an internal-wave energy of 4×10^6 ergs cm^{-2} (Garrett and Munk, 1979), a flux of energy to the boundary layer of 0.01 erg cm^{-2} s^{-1} will absorb all the energy in the internal-wave field in roughly 12 years. Estimates of the energy flux into the internal-wave field generally yield turnover times smaller than this by an order of magnitude or more (Käse, 1979; Fu, 1981; Bell, 1975). Unless these estimates are grossly wrong, the benthic boundary layer over a flat bottom plays a minor role in the internal-wave energy budget.

Acknowledgments. I would like to thank Laurence Armi for innumerable discussions and many valuable suggestions. Discussions with M. Briscoe, D. Caldwell, R. Davis, W. Owens, E. Mollo-Christensen and R. Weller have been helpful. G. Weatherly provided some unpublished data. I thank one of the referees for pointing out the importance of diurnal tides. This research was supported by the Office of Naval Research under Contract N00014-76-C-0197, NR 083-400 and the National Science Foundation under Grant OCE 76-81190 through the Woods Hole Oceanographic Institution. Partial support was provided by a National Science Foundation graduate fellowship. Publication costs were supported by the Office of Naval Research under Contracts N00014-80-C-0252 through the Applied Physics Laboratory, University of Washington and N00014-80-C-0440 through the Scripps Institution of Oceanography. This is contribution number 4877 from the Woods Hole Oceanographic Institution.

APPENDIX

Eq. (17), Third Term

The third term in (17) cannot be evaluated from the current-meter data, so its magnitude is here estimated and shown to be small. The total energy flux per unit area due to this term is

$$D = \int_0^{z_r} \hat{w}^\dagger(z) \frac{\partial \overline{\hat{w}'^2}}{\partial z} dz, \qquad (1A)$$

where $\hat{w}(z)$ is strongly constrained by the condition $\hat{w}(0) = 0$ and by $\hat{w}(z_r)$, the latter being due solely to internal waves. $\overline{\hat{w}'^2}$ will not be larger than $u^{*2} \approx (U/30)^2$. Thus an upper bound for (1A) is

$$D < |\hat{w}(z_r)|\, u^{*2}. \qquad (2A)$$

For internal waves (Fofonoff, 1969)

$$\frac{|\hat{w}|^2}{|\hat{u}|^2 + |\hat{v}|^2} = \frac{\sigma^2}{N^2} \frac{\sigma^2 - f^2}{\sigma^2 + f^2}. \qquad (3A)$$

Fu (1981) shows that because of turning-point effects, this expression is only valid for $\sigma > 1.02f$; for smaller $\sigma - f$, $|\hat{w}|^2$ is bounded above by (3A) with $\sigma = 1.3f$. Using $\sigma = 1.3f$, $\sigma = 0.1N$, $|\hat{u}|^2 + |\hat{v}|^2 = 1$ cm^2 s^{-2}, $U = 7$ cm s^{-1} yields

$$D < 0.0027 \text{ erg cm}^{-2} \text{ s}^{-1}, \qquad (4A)$$

which is less than 20% of the total calculated energy absorption from the clockwise term in (18).

REFERENCES

Armi, L., and E. D'Asaro, 1980: Flow structures of the benthic ocean. *J. Geophys. Res.*, **85,** 469–483.

Bell, T. H., Jr., 1975: Topographically generated internal waves in the ocean. *J. Geophys. Res.*, **80,** 320–327.

Bowden, K. F., 1978: Physical problems of the benthic boundary layer. *Geophys. Surv.*, **3,** 255–296.

D'Asaro, E., 1978: Mixed layer velocities induced by internal waves. *J. Geophys. Res.*, **83,** 2437–2438.

——, 1980: Structure and dynamics of the benthic boundary layer above the Hatteras Abyssal Plain. Ph.D. thesis, MIT/WHOI Joint Program in Oceanography.

——, 1982: Velocity Structure of the benthic ocean. *J. Phys. Oceanogr.*, **12,** 313–322.

Fofonoff, N. P., 1969: Spectral characteristics of internal waves in the ocean. *Deep-Sea Res.*, **16,** 59–71.

Fu, L. L., 1981: Observations and models of inertial waves in the deep ocean. *Rev. Geophys. Space Phys.*, **19,** 141–170.

Garrett, C. J. R., and W. Munk, 1975: Space-time scales of internal waves: a progress report. *J. Geophys. Res.*, **80,** 291–297.

——, and ——, 1979: Internal waves in the ocean. *Annual Review of Fluid Mechanics*, Vol. 11, Annual Reviews, Inc., 339–369.

Greenspan, H. P., 1968: *The Theory of Rotating Fluids.* Cambridge University Press, 327 pp.

Gregg, M. C., and M. G. Briscoe, 1979: Internal waves, fine-structure, microstructure and mixing in the ocean. *Rev. Geophys. Space Phys.*, **17,** 1524–1548.

Harris, F. J., 1978: On the use of windows for harmonic analysis with the discrete fast Fourier transform. *Proc. IEEE,* **66,** 51–83.

Käse, R. H., 1979: Calculations of the energy transfer by the wind to near-inertial waves. *Deep-Sea Res.*, **26,** 227–232.

Koopmans, L. H., 1974: *The Spectral Analysis of Time Series.* Academic Press.

Kundu, P. K., 1976: An analysis of inertial oscillations observed near Oregon coast. *J. Phys. Oceanogr.*, **6,** 879–893.

Leaman, K. D., 1976: Observations on the vertical polarization and energy flux of near-inertial waves. *J. Phys. Oceanogr.*, **6,** 894–908.

Lighthill, J., 1978: *Waves in Fluids.* Cambridge University Press, 504 pp., (see Chap. 4).

McComas, C. H., 1977: Equilibrium mechanisms within the oceanic internal wave field. *J. Phys. Oceanogr.*, **7,** 836–845.

Müller, P., D. J. Olbers and J. Willebrand, 1978: The IWEX spectrum. *J. Geophys. Res.*, **83,** 479–500.

Munk, W., and N. Phillips, 1968: Coherence and band structure of inertial motion in the sea. *Rev. Geophys.*, **6,** 447–472.

——, F. Snodgrass and M. Wimbush, 1970: Tides off-shore: Transition from California coastal to deep-sea waters. *Geophys. Fluid Dyn.*, **1,** 191–235.

Phillips, O. M., 1977: *The Dynamics of the Upper Ocean*, 2nd ed. Cambridge University Press, 336 pp.

Priestley, C. H. B., 1959: *Turbulent Transfer in the Lower Atmosphere*. The University of Chicago Press, 130 pp.

Rhines, P. B., 1979: Geostrophic turbulence. *Annual Reviews of Fluid Mechanics*, Vol. 11, Annual Reviews, Inc., 401–441.

Sanford, T., 1975: Observations of the vertical structure of internal waves. *J. Geophys. Res.*, **80,** 3861–3871.

Schmitz, W. J., Jr., 1976: Eddy kinetic energy in the deep western North Atlantic. *J. Geophys. Res.*, **81,** 4981–4982.

Spencer, A., E. D'Asaro and L. Arml, 1981: The Benthic Boundary Layer Experiment on the Hattaras Abyssal Plain: Current and temperature observations. Woods Hole Oceanographic Institution, Tech. Rep. WHOI-1981-12.

Tennekes, H., and L. L. Lumley, 1972: *A First Course in Turbulence*. The MIT Press, 300 pp.

Townsend, A. A., 1965: Excitation of internal waves by a turbulent boundary layer. *J. Fluid Mech.*, **22,** 241–252.

Weatherly, G. L., 1972: A study of the bottom boundary layer of the Florida Current. *J. Phys. Oceanogr.*, **2,** 54–72.

——, and M. Wimbush, 1980: Near bottom speed and temperature observations on the Blake-Bahama Outer Ridge. *J. Geophys. Res.*, **85,** 3971–3981.

Zetler, B., W. Munk, H. Mofjeld, W. Brown and F. Dormer, 1975: MODE tides. *J. Phys. Oceanogr.*, **5,** 430–441.